Florence, Italy 12-16 July 2015
ICSV22
The 22nd International Congress on Sound and Vibration

THE EFFECT OF VERTICAL-LATERAL COUPLING OF RAILS INCLUDING INITIAL CURVATURE

Dimitrios Kostovasilis, David J. Thompson
Institute of Sound and Vibration Research, University of Southampton, Highfield Campus, Southampton, SO17 1BJ, United Kingdom
email: d.kostovasilis@soton.ac.uk

Mohammed F.M. Hussein
Civil and Architectural Engineering Department, Qatar University, P.O. Box 2713, Qatar

An understanding of the dynamic behaviour of railway tracks at high frequencies, in both vertical and lateral directions, is important for the assessment of rolling noise. Although many analytical models can be found in the literature, these mostly focus on the vertical vibration of the track. Studies of the lateral vibration are less common while the coupling between the vertical and lateral directions has received very little attention. In this paper, a model of a beam on an elastic foundation is introduced that accounts for the coupling of the vertical and lateral vibration behaviour. The model allows for the effects of beam curvature, asymmetry of the cross-section, shear deformation, rotary inertia and warping. Consideration is given to the fact that the loads at the rail head, as well as those exerted by the railpads at the rail foot, may not be applied through the centroid of the section. The track is subjected to a non-moving harmonic load and the solution is obtained in the wavenumber domain using the Fourier transform method. Results are presented as dispersion curves for the free rail and are validated with the aid of a Finite Element software. Closed form analytical expressions are derived, using contour integration, for the forced response. The track vibration decay rates are also presented and analysed as a means of assessing the noise performance of the rail and the influence of vertical-lateral coupling.

1. Introduction

The dynamic behaviour of railway tracks at high frequencies and their radiation characteristics are particularly important for the generation of rolling noise. The track vibration in both vertical and lateral directions is important. Many analytical models can be found in the literature that focus on vertical track vibration but lateral vibration and especially the coupling of the vertical and lateral directions have received much less attention.

The cross-section of the rail is asymmetric in the vertical direction. As a result, the shear centre, through which the shear forces act, is not coincident with the centroid through which inertial forces act. This introduces coupling between lateral bending and torsion. For a fully asymmetric section, such as a tram groove rail, the same will occur between vertical bending and torsion. In addition, in a curved track the vertical bending will couple with the torsion and the lateral bending with the axial response.

Grassie et al. [1] modelled lateral track dynamics using similar models to those used for the vertical direction, neglecting coupling. In [2], both vertical and lateral track behaviour was again considered using a Timoshenko beam on a two-layer foundation model. Although the vertical/lateral coupling was not taken into account directly, an empirical parameter was introduced (X) for the cross-coupling. The cross receptance was estimated from the geometrical average of the vertical (A_x) and lateral (A_y) receptances ($A_{xy} = X\sqrt{A_x A_y}$), where X was obtained by comparison with measurements.

In [3] and [4] continuously supported multiple beam models were developed, including cross-sectional deformation, for both vertical and lateral motion. Although they show excellent agreement with a Finite Element (FE) model, the effect of vertical-lateral coupling was not considered.

Since the cross-sectional deformations are important in the frequency range of interest, various more detailed models have been developed that are based on extensions of the FE method, eg [5, 6]. In [7], the dispersion relationship and receptance of an infinite rail were presented, based on an FE model using periodic structure theory.

In the present work, an analytical approach is used to consider the various sources of vertical/lateral interaction although cross-section deformation is not taken fully into account. The rail is treated as a simple beam cross-section, accounting for vertical and lateral bending and torsion. Corrections for shear deformation, shear centre eccentricity and warping are included as well as coupling through track curvature. The dispersion curves are compared with results from a FE model. The potential effects of the various sources of vertical/lateral coupling on rolling noise are presented in terms of track decay rates. The main aim of this work is to provide insight into the various coupling effects that exist for railway applications, and their importance in modelling.

2. Coupled vertical/lateral interaction model

The dynamic track model is based on a beam model presented by Kim et al. [8]. This utilises Timoshenko beam theory for bending in the vertical and lateral directions, an axial rod in tension and a torsional rod accounting for non-uniform torsion. Figure 1 shows a typical rail cross-section, where C denotes the centroid and S the shear centre; e_2 is the distance between them.

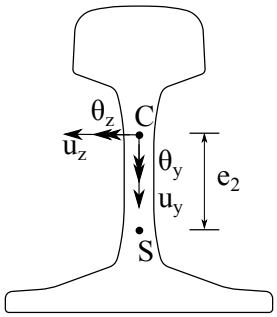

Figure 1: Displacement field

Based on the generalised displacement field in the cross-section of the rail, the strains are derived. In Fig. 2 an infinitesimal element of length $Rd\theta$ is presented, along with the forces acting on it (excluding the bi-moment which is associated with warping). By summing the forces and moments

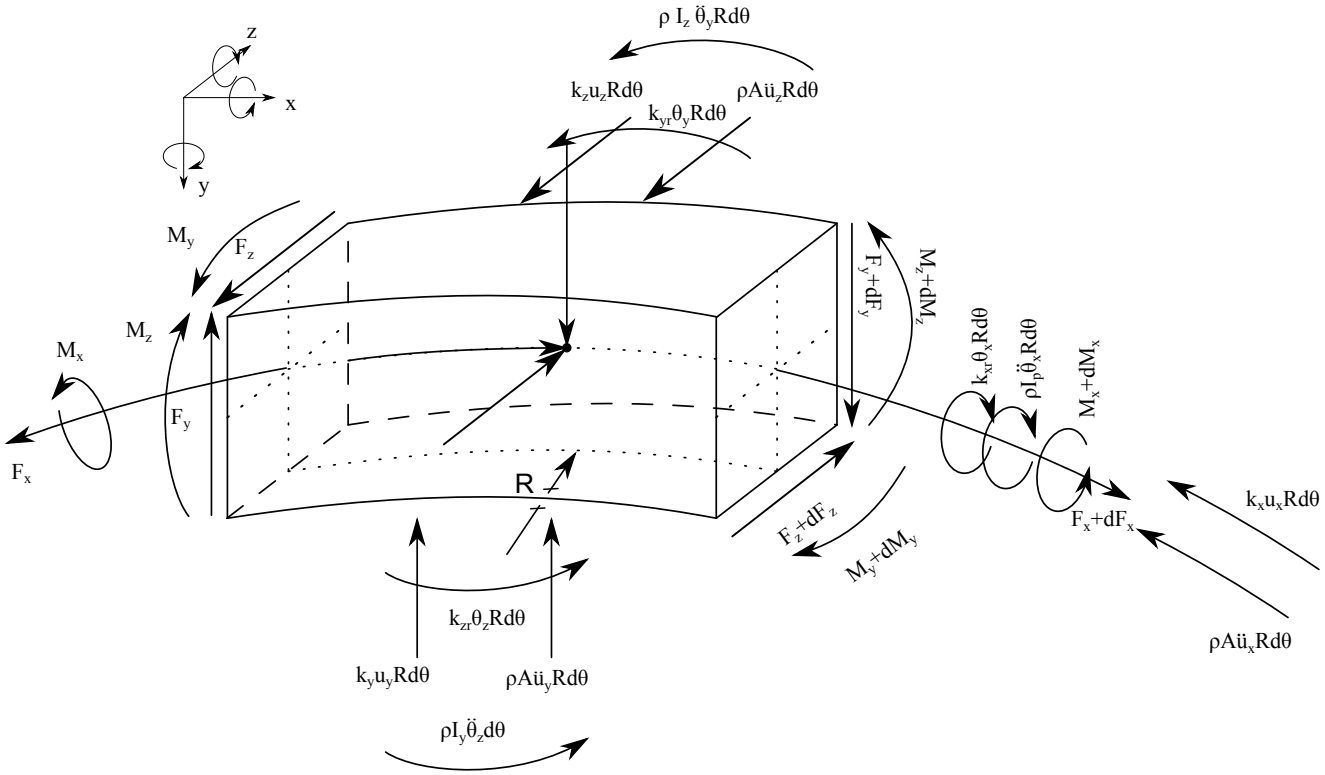

Figure 2: Infinitesimal element

acting on the centroid in all three directions, the following equations of motion are obtained:

$$-\frac{1}{R}\frac{dF_x}{d\theta} - \frac{F_z}{R} + k_x u_x + m\ddot{u}_x = \tilde{F}_x \tag{1}$$

$$-\frac{1}{R}\frac{dF_y}{d\theta} + k_y u_y + m\ddot{u}_y = \tilde{F}_y \tag{2}$$

$$-\frac{1}{R}\frac{dF_z}{d\theta} + \frac{F_x}{R} + k_z u_z + m\ddot{u}_z = \tilde{F}_z \tag{3}$$

$$-\frac{1}{R}\frac{dM_x}{d\theta} + \frac{M_z}{R} + \rho I_p \ddot{\theta}_x + k_{xr}\theta_x = \tilde{M}_x \tag{4}$$

$$-\frac{1}{R}\frac{dM_y}{d\theta} + F_z + \rho(I_z - I_{wy})\ddot{\theta}_y - \rho I_{yz}\ddot{\theta}_z + k_{yr}\theta_y + I_{wz}\rho\ddot{f} = \tilde{M}_y \tag{5}$$

$$\frac{1}{R}\frac{dM_z}{d\theta} + \frac{M_x}{R} - F_y + \rho(I_y + I_{wz})\ddot{\theta}_z - \rho I_{yz}\ddot{\theta}_y + k_{zr}\theta_z - I_{wy}\rho\ddot{f} = \tilde{M}_z \tag{6}$$

$$-\frac{1}{R}\frac{dM_w}{d\theta} + T_w + \rho I_w \ddot{f}_w - \rho I_{wz}\ddot{\theta}_z + \rho I_{wy}\ddot{\theta}_y = \tilde{M}_w \tag{7}$$

where u_x and θ_x are the displacement and rotation in the x direction, F_x and M_x are the internal forces and moments acting in the x direction, and similarly for the y and z directions. M_w is the bi-moment and T_w is the non-uniform torsion component, k_x and k_{xr} etc represent the foundation stiffness per unit length for displacements and rotations respectively, R is the radius for a curved beam, $m = \rho A$ is the beam mass per unit length, I is the second moment of area about the respective axis, $\tilde{F}_x$, $\tilde{F}_y$, $\tilde{F}_z$, $\tilde{M}_x$, $\tilde{M}_y$, $\tilde{M}_z$ and $\tilde{M}_w$ are the external forces per unit length due to the excitation source.

Based on the equations of motion, the strain-displacement equations for the beam can be obtained. Then the axial strain (ϵ_{xx}) and the shear strains (γ_{xy} and γ_{xz}) can be written in terms of the displacement (e.g. [8]). By taking the appropriate integrals of the normal and shear strains over the cross-section, the force-deformation equations are obtained. The responses are then assumed to be harmonic both in space and time with a complex amplitude. For example, the axial response u_x is expressed as

$u_x = U_x e^{i\omega t} e^{-i\xi x}$ where U_x denotes the complex amplitude. By substituting this form of response back into Eqs. 1 - 7 and collecting terms for the complex amplitudes the following is obtained:

$$\mathbf{A}(\xi, \omega)\bar{\mathbf{U}} = \mathbf{F}(\xi, \omega) \tag{8}$$

where $\bar{\mathbf{U}}$ contains the complex amplitudes, $\mathbf{F}$ the forces and the dynamic stiffness matrix $\mathbf{A}$ is a 7-by-7 matrix of coefficients dependent on ξ and ω. Now by collecting terms within $\mathbf{A}$ for ascending powers of ξ, it follows that:

$$\left(\left(\mathbf{K}_0 - \omega^2\mathbf{M}\right)\xi^0 - i\xi\mathbf{K}_1 - \xi^2\mathbf{K}_2\right)\bar{\mathbf{U}} = \mathbf{F}(\xi, \omega) \tag{9}$$

In order to obtain the dispersion relationship, the free vibration of the rail ($\mathbf{F}(\xi, \omega) = \mathbf{0}$) is considered. For such a case, non-trivial solutions require $|\mathbf{A}| = 0$. This is a dual (non-linear) eigenvalue problem in ξ and ω. In order to simplify the solution process, the 7-by-7 non-linear eigenvalue problem is rewritten as an equivalent 14-by-14 linear eigenvalue problem, yielding 14 solutions for ξ at each frequency (7 in each direction) [9].

3. Validation for a free rail

In order to validate the above model, a FE model was developed in order to obtain the dispersion relations for a free beam and compare against the developed model. Tetrahedral solid elements of maximum side length of 0.066 m were used. Figures 3 and 4 show the dispersion relationship for a straight and curved beam respectively, based on the properties shown in Table 1 obtained through analysing the cross-section in the FE model.

Table 1: Properties of rail.

Parameter	Value	Parameter	Value
Cross-section area, A	7.67×10^{-3} m^2	Young's modulus, E	200 GPa
Moment of inertia, I_z	3038×10^{-8} m^4	Shear modulus, G	76.923 GPa
Moment of inertia, I_y	512.7×10^{-8} m^4	Polar mom. of inertia, I_p	3.550×10^{-5} m^4
Torsional constant, J	2.212×10^{-6} m^4	Density, ρ	7860 kg/m^3
Shear coefficient, κ_y	0.39	Shear coefficient, κ_z	0.54
Shear centre distance, e_2	0.033 m	Sectorial mom. of inertia, I_w	2.212×10^{-8} m^6
Product of inertia, I_{yz}	0 m^4	Product of inertia, I_{wz}	-8.046×10^{-15} m^5
Product of inertia, I_{wy}	0 m^5	Rail loss factor, η_r	0.02

In Fig. 3 the FE results are plotted for a straight rail of length 1.2 m with symmetry or anti-symmetry boundary conditions at each end. The lateral (red) and vertical-longitudinal (green) motions are uncoupled for a straight rail. The vertical motion includes two main wave-types. The first is the vertical bending (Type I) while the second is a higher-order wave associated with the foot flapping (Type II). Longitudinal waves include the first order axial wave (Type III) and a higher order axial wave (Type IV). For the lateral motion of the rail, the first two wave types correspond to the lateral bending (Type I) and the torsional wave (Type II). Two higher-order waves appear at higher frequencies, corresponding to the bending (Type III) and double bending (Type IV) of the web.

Because the cross-section geometry is not included in the present model (i.e. no separation of head, web and flange) the higher order wave-types are not accounted for and therefore their effects are not present. This also means that the lateral bending wave, for example, above 200 Hz does not match that of the FE model since in the latter case it is influenced by the cross-section deformation.

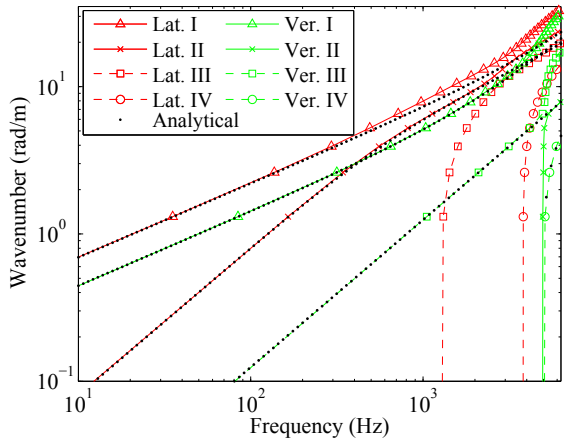

Figure 3: Comparison of dispersion curves for straight rail with FE model

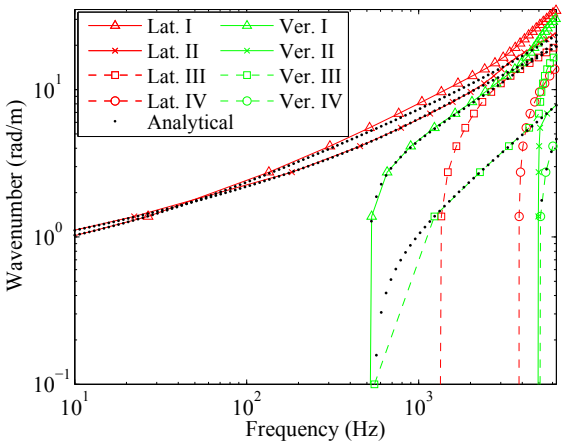

Figure 4: Comparison of dispersion curves for curved rail with FE model ($R = 1.45$ m)

The added flexibility in the web in the FE model, causes waves to travel at higher wavenumbers, leading to the deviations of the analytical model from the FE model at high frequencies. Similarly, the torsional wave (lateral wave type II) is seen to be influenced by the web bending in the FE model at higher frequencies.

The dispersion relationship for a curved beam of radius 1.45 m is plotted in Fig. 4. Although this radius is unrealistic for railway applications, it is used here for the validation of the model and to emphasize the effect of curvature. It can be seen that the main differences from a straight rail occur below about 1500 Hz. The most obvious difference is that two of the waves, namely the first longitudinal and second lateral wave types, cut on at around 500 Hz (550 and 510 Hz respectively), whereas for a straight rail they cut on at 0 Hz.

The cut-on frequency of the first order longitudinal wave is most commonly referred to as the breathing or ring mode. In this mode, the ring expands and contracts in the radial direction uniformly. It can seen as a lateral movement of the cross-section, but since this is uniform throughout the curved beam, the axis of the beam extends/contracts, thus making the beam centreline longer/shorter. The frequency is identified analytically as (e.g. [10]):

$$f_{co,1} = \frac{1}{2\pi R}\sqrt{\frac{E}{\rho}} \tag{10}$$

The second mode is similar to the rigid-body torsional mode for a straight beam. This is related to the uniform rotation of the ring cross-section about the shear centre. It corresponds to a rigid-body mode of the beam in torsion for a straight beam, but for a curved beam it will include bending in the vertical direction, as the beam rotates [11]. This cuts on at the following frequency:

$$f_{co,2} = \frac{1}{2\pi R}\sqrt{\frac{EI_z}{\rho I_p}} \tag{11}$$

It is seen that this mode does not depend on the torsional rigidity as no relative torsion takes place, but rather on the bending stiffness of the beam and the polar moment of inertia.

4. Closed form solution for the response

To obtain the forced response, Equation 8 is solved for the unknown response, giving:

$$\bar{\mathbf{U}} = \mathbf{A}^{-1}\mathbf{F} = \frac{\mathbf{B}_1(\xi,\omega)}{\mathbf{B}_2(\xi,\omega)} \tag{12}$$

where $\mathbf{B}_1(\xi,\omega) = adj(\mathbf{A})\mathbf{F}$ and $\mathbf{B}_2(\xi,\omega) = det(\mathbf{A})$. Taking the inverse Fourier transform over wavenumber:

$$\mathbf{U}(x) = \frac{1}{2\pi}\int_{-\infty}^{\infty}\frac{\mathbf{B}_1(\xi,\omega)}{\mathbf{B}_2(\xi,\omega)}e^{-i\xi x}d\xi \tag{13}$$

The above integration is performed using contour integration [12] and is evaluated as:

$$\mathbf{U}(x) = -\mathrm{i}\sum_{n=1}^{N} e^{-i\xi_n x} Res\left[B(\xi,\omega),\xi_n\right] \tag{14}$$

where ξ_n are the poles in the upper (or lower) half-plane (depending on the sign of x), $B(\xi,\omega) = B_1(\xi,\omega)/B_2(\xi,\omega)$ and the residues are given by:

$$Res\left[B(\xi,\omega),\xi_n\right] = B_1(\xi_n,\omega)/B_2'(\xi_n,\omega) \tag{15}$$

with the dash ($'$) meaning the derivative with respect to ξ.

5. Decay rates and mobility

In this section, results are presented of the overall track decay rate, calculated from the forced response. Results for both vertical and lateral track decay rates are presented for a typical ballasted railway track, properties of which are listed in Table 2.

Table 2: Properties of track.

Parameter	Value	Parameter	Value
Railpad vertical stiffness, k_y	120 MN/m/m	Railpad lateral stiffness, k_z	40 MN/m/m
Railpad axial stiffness, k_x	40 MN/m/m	Pad loss factor, η_p	0.1
Railpad width (rail foot), w_f	150 mm	Foot to centroid distance, y_f	81 mm

The decay rate (dB/m) in each one-third octave band is evaluated as [13]:

$$\Delta = \frac{4.343}{\sum_{x=0}^{x_{max}}\frac{|A(x_n)|^2}{|A(x_0)|^2}\delta x_n} \tag{16}$$

where $A(x_n)$ is the calculated mobility in the one-third octave band at a location x_n away, $A(x_0)$ is the mobility of the excitation point and δx_n is the length of rail segment associated with the point x_n.

To calculate the vertical response, the rail is excited 20 mm from the centre of the railhead and the response is obtained at the same position at various distances x_n. The decay rate and mobility for the vertical excitation are plotted in Fig. 5. Equivalent results are shown in Fig. 6 for the lateral excitation, where the force and response points are located 20 mm below the top of the railhead. The black line represents the classical Timoshenko beam model, the magenta line represents the current model without accounting for shear-centre eccentricity or warping, the green and red lines show only the individual effect of shear centre eccentricity and warping respectively, while the blue line represents the fully coupled model. Finally the cyan line is for a curved rail with $R = 100$ m.

At low frequencies, the decay rates are high due to the blocking effect of the support. They drop around the cut-off frequency of the rail bouncing on the railpad ($\sqrt{k_y/m}/2\pi$). At high frequencies, the decay rate increases due to damping in the rail (ie $E = E(1 + i\eta_r)$). Similar behaviour is observed for

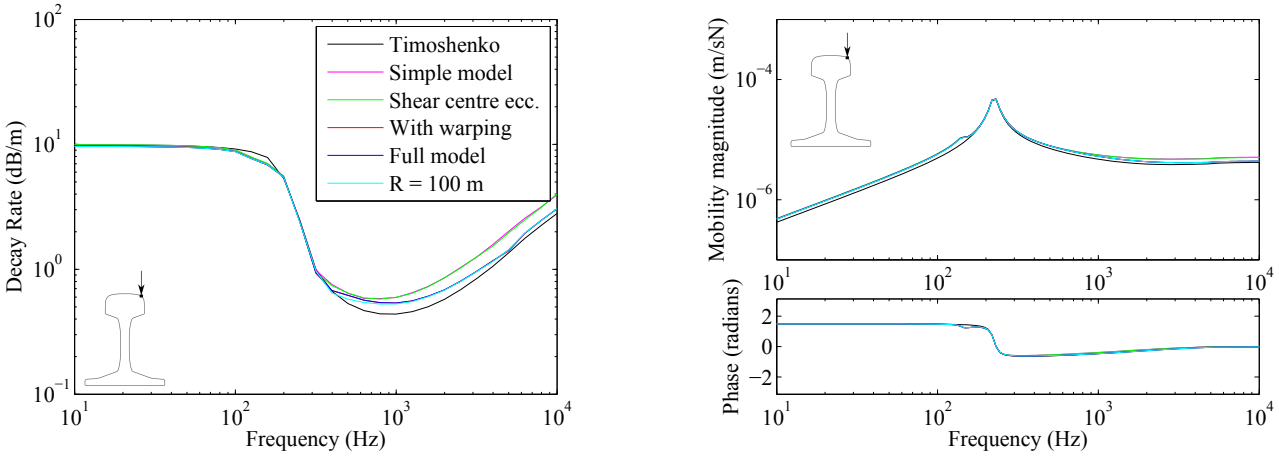

Figure 5: Track decay rate and mobility for vertical excitation

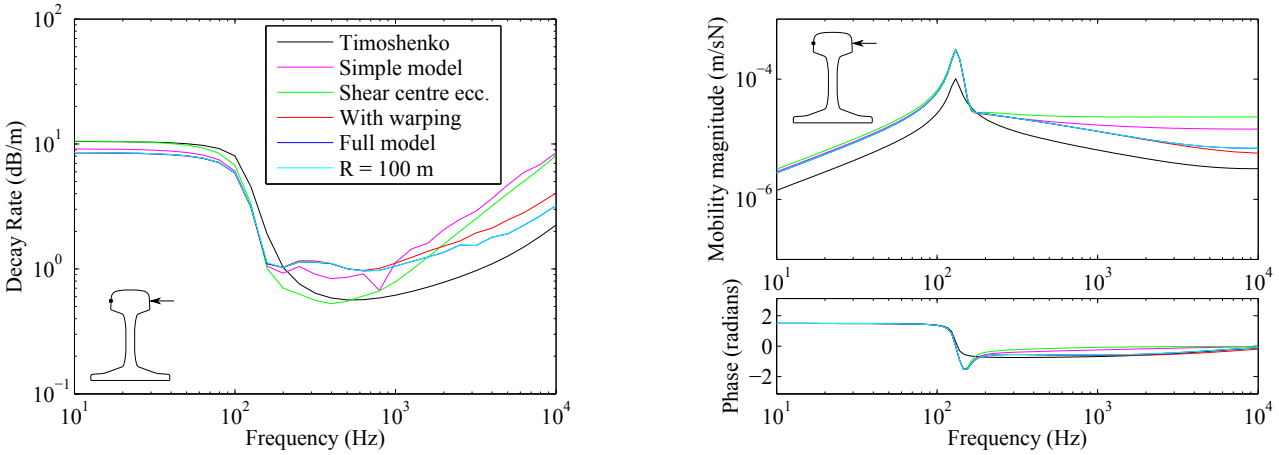

Figure 6: Track decay rate and mobility for lateral excitation

the lateral direction, with the decay rate dropping at a lower frequency due to the smaller foundation stiffness.

For the vertical case, changes are seen due to the eccentric applied load exciting the torsional response as well as the lateral. This is due to the change in input mobility $A(x_0)$ whereas the decay rate of the torsional wave is higher than that of the bending wave, thus at a distance from the excitation source, the response is mainly influenced by the bending behaviour. If the rail is excited through its centreline all six curves would be identical. A peak is seen in the mobility at about 140 Hz, which corresponds to the cut-off frequency ($\sqrt{k_{xr}/(\rho I_p)}/2\pi = 143$ Hz) of torsional waves; the torsional pad stiffness is given by $k_{xr} = w_f^2 k_y/12$, where w_f is the width of the railfoot and k_y is the vertical stiffness. At higher frequencies, the decay rate is mainly influenced by changes in the mobility.

Similar observations can be made for the lateral case. Overall, the difference in mobility relative to the classical Timoshenko beam model is higher than for the vertical bending, as the effect of torsion is more influential in the lateral response. The cut-off frequency of the rail bouncing on the railpad (130 Hz) and that of the torsional wave (143 Hz) are very close and thus are not seen as two independent peaks. In addition, the cross-section is asymmetric relative to the horizontal axis, thus providing a further coupling between the lateral bending motion and torsion.

For both vertical and lateral directions, the effect of curvature is seen to be insignificant for the radius considered here. Since typical railway tracks will mostly have curvatures greater than this, it

can be concluded that track curvature is not an important aspect in modelling the response of curved rails. Instead, a straight rail model is sufficient and should be preferred to avoid added complexity.

6. Conclusion

An improved model for prediction of the response of a railway track is presented. The effects of shear centre eccentricity, warping and curvature of the track have been included. The model is validated for the case of a free rail against an FE model, providing excellent agreement up to 2 kHz. For a supported rail, results for the track decay rate and point mobility are presented for both vertical and lateral excitation.

The response in both the vertical and lateral directions is mostly influenced by the inclusion of torsion in the model. The effect of curvature is found to be minimal for the modelling of rails, and instead a straight rail model is sufficient. In order to improve the model further for higher frequencies, consideration needs to be given to the cross-sectional deformation which is especially significant for the lateral response.

REFERENCES

1. Grassie, S.L., Gregory, R.W., and Johnson, K.L. The dynamic response of railway track to high frequency lateral excitation. *Journal of Mechanical Engineering Science*, 24(2):91–95, (1982).

2. Thompson, D.J., Hemsworth, B., and Vincent, N. Experimental validation of the TWINS prediction program for rolling noise, Part 1: Description of the model and method. *Journal of Sound and Vibration*, 193 (1):123–135, (1996).

3. Wu, T.X., and Thompson, D.J. A double Timoshenko beam model for vertical vibration analysis of railway track at high frequencies. *Journal of Sound and Vibration*, 224(2):329–348, (1999).

4. Wu, T.X., and Thompson, D.J. Analysis of lateral vibration behavior of railway track at high frequencies using a continuously supported multiple beam model. *The Journal of the Acoustical Society of America*, 106(3):1369–1376, (1999).

5. Gavrić, L. Computation of propagative waves in free rail using a finite element technique. *Journal of Sound and Vibration*, 185:531–543, (1995).

6. Gry, L. Dynamic modelling of railway track based on wave propagation. *Journal of Sound and Vibration*, 195:477–505, (1996).

7. Thompson, D.J. Wheel-rail noise generation, Part III: Rail vibration. *Journal of Sound and Vibration*, 161 (3):421–446, (1993).

8. Kim, M.Y., Kim, N.I., and Kim S.B. Spatial stability of shear deformable curved beams with non-symmetric thin-walled sections. I: Stability formulation and closed-form solutions. *Computers and Structures*, 83:2525–2541, (2005).

9. Tisseur, F., and Meerbergen, K. The quadratic eigenvalue problem. *SIAM Review*, 43(2):235–286, (2001).

10. Rao, S.S., *Vibration of continuous systems*. New Jersey: John Wiley & Sons, Inc., (2007).

11. Basset, A.B. On the theory of elastic wires. *Proceedings of the London Mathematical Society*, 105(27): 105–127, (1891).

12. Wunsch, D.A., *Complex variables with applications*. Pearson Addison-Wesley, (2006).

13. BS EN 15461:2008+A1 *Railway applications - Noise emission - Characterization of the dynamic properties of track selections for pass by noise measurements*, (2010).